DOI: 10.1021/ma101646r

Macromolecules
ARTICLE

A Tale of Current and Voltage: Interplay of Band Gap and Energy Levels of Conjugated Polymers in Bulk Heterojunction Solar Cells

Huaxing Zhou,[†] Liqiang Yang,[‡] Shubin Liu,[§] and Wei You*[,†,‡]

[†]*Department of Chemistry, University of North Carolina at Chapel Hill, Chapel Hill, North Carolina 27599-3290, United States,* [‡]*Curriculum in Applied Sciences and Engineering, University of North Carolina at Chapel Hill, Chapel Hill, North Carolina 27599-3287, United States, and* [§]*Research Computing Center, University of North Carolina at Chapel Hill, Chapel Hill, North Carolina 25599-3420, United States*

Received May 7, 2010; Revised Manuscript Received October 19, 2010

ABSTRACT: We recently proposed a design strategy of "weak donor−strong acceptor" copolymer to approach ideal polymers with both a low HOMO energy level and a small band gap for bulk heterojunction (BHJ) polymer solar cells in order to achieve both a high open circuit voltage (V_{oc}) and a high short circuit current (J_{sc}) [*ACS Appl. Mater. Interfaces* **2010**, *2*, 1377]. To further demonstrate the delicate interplay of the V_{oc} and J_{sc} through molecular design of conjugated polymers, two such "weak donors", naphtho[2,1-*b*:3,4-*b*′]-dithiophene (NDT) and dithieno[3,2-*f*:2′,3′-*h*]quinoxaline (QDT), which differ only by two atoms, were copolymerized with a common acceptor, 4,7-di(2-thienyl)-2,1,3-benzothiadiazole (DTBT). The BHJ devices based on PNDT−4DTBT and PQDT−4DTBT as the donor polymer (with $PC_{61}BM$ as the acceptor) exhibit overall efficiencies of 5.1% and 4.3%, respectively. Through these two structurally related polymers, we demonstrate that incorporating electron-withdrawing atoms in the *donor unit* would lead to a lower HOMO energy level. This lower HOMO energy level translates into a higher open circuit voltage (V_{oc}) of 0.83 V in PQDT−4DTBT-based BHJ devices. In contrast, the slightly higher HOMO energy level (− 5.34 eV) of PNDT−4DTBT limits the V_{oc} to 0.67 V. Since the LUMO levels of both polymers are similar, the higher HOMO energy level of PNDT−4DTBT leads to a smaller band gap of 1.61 eV (vs 1.70 eV of PQDT−4DTBT), which contributes to a noticeably higher J_{sc} of 14.20 mA/cm^2 (vs 11.38 mA/cm^2 of PQDT−4DTBT-based BHJ devices). Future research needs to focus on the employment of even weaker donor and stronger acceptors via innovative structural modification in order to *concurrently* achieve a deeper HOMO and a lower band gap, thereby enhancing *both* V_{oc} and J_{sc}.

Introduction

Anticipated to be low-cost alternatives to existing silicon photovoltaics, polymer-based bulk heterojunction (BHJ) solar cells have not yet delivered their promise due to persistently low efficiencies.[1−3] However, rapid progress has been made recently with efficiencies as high as 7% being reported.[4,5] In order to achieve their predicted 10% efficiency,[6] the structure and function relationship of these polymers needs to be better understood. Therefore, thorough studies of structurally related polymers must be performed to help clearly define future design rationale.

Two equally important parameters in determining the efficiency of any given solar cell are open circuit voltage (V_{oc}) and short circuit current (J_{sc}). In polymer BHJ solar cells, the V_{oc} and J_{sc} are largely influenced by the energy level and band gap of the conjugated polymers. As the benchmark for BHJ solar cells, poly(3-hexylthiophene) (P3HT) provides a V_{oc} of ∼0.6 V with a HOMO level of −5.1 eV and a J_{sc} of ∼11 mA/cm^2 at a band gap of 1.9 eV.[1] In order to increase the V_{oc} of P3HT, structural units with a high oxidation potential such as carbazole,[7] fluorene,[8] ladder-type *p*-phenylene,[9] and silafluorene[10] have been employed to construct low band gap polymers via the donor−acceptor approach. This has successfully yielded V_{oc} as high as 1 V in related BHJ devices.[8,9] Unfortunately, insufficient light absorption resulted from their relatively large band gaps (> 1.8 eV) limits the J_{sc} to less than 11 mA/cm^2, even with internal quantum efficiency approaching 100%.[7] Alternatively, by constructing polymers with much smaller band gaps through structural moieties such as cyclopentadithiophene (or its silol version)[11] and thienothiophene,[12,13] the J_{sc} can be enhanced to as high as 17 mA/cm^2.[11] However, the V_{oc} of related devices is often lower than 0.6 V[11,12] due to an elevated HOMO energy level.

Recognizing the importance of achieving both a high V_{oc} and a high J_{sc}, the community of polymer solar cells has created a number of high performing low band gap polymers with deep HOMO levels.[5,7,9,14−19] A "weak donor−strong acceptor" strategy was thereby proposed to *concurrently* lower the HOMO energy level and the band gap.[20] One such copolymer, PNDT−BT, incorporating naphtho[2,1-*b*:3,4-*b*′]dithiophene and benzothiadiazole (BT), indeed demonstrated both a low HOMO energy level of −5.35 eV and a low band gap of 1.64 V. Though a noticeably high V_{oc} of 0.83 V was obtained from the BHJ device of PNDT−BT blended with $PC_{61}BM$, the J_{sc} was only 2.90 mA/cm^2, attributed to the low molecular weight and low hole mobility of PNDT−BT. Later, we show that 4,7-di(4-hexyl-2-thienyl)-2,1,3-benzothiadiazole (4DTBT) can impart low band gap polymers with improved solubility and (thereby) high molecular weight.[21]

Therefore, a new polymer, PNDT−4DTBT, was envisioned and synthesized (Figure 1). BHJ solar cells based on the blend of this polymer and $PC_{61}BM$ demonstrated a V_{oc} of 0.67 V, a J_{sc} of 14.20 mA/cm^2, and a *FF* of 0.54, yielding an overall efficiency of 5.1% under 1 sun condition (AM 1.5, 100 mW/cm^2). In order to improve the V_{oc} by further lowering the HOMO energy level, we substituted the two C atoms of the center naphthalene unit within

*To whom all correspondence should be addressed. E-mail: wyou@email.unc.edu.

 Published on Web 11/19/2010

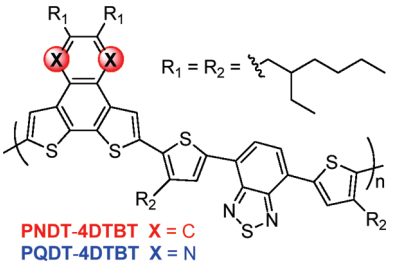

Figure 1. Structure of polymers. (i) Naphthalene/quinoxaline center ring lowers oxidation potential, and planarity of NDT/QDT unit encourages crystallinity. (ii) Additional alkylated positions (R_2) ensure high molecular weight and soluble polymers without introducing severe steric hindrance between donor (NDT/QDT) and acceptor (4DTBT).

NDT with two nitrogen atoms, converting NDT into an even *weaker* donor, dithieno[3,2-*f*:2′,3′-*h*]quinoxaline (QDT).[22] As expected, PQDT−4DTBT offered a much improved V_{oc} of 0.83 V. Interestingly, a similar overall efficiency was obtained (4.3%), largely due to a noticeably deceased J_{sc} (11.4 mA/cm^2). Comparison of these two structurally related polymers has set an excellent example to demonstrate the delicate interplay between the HOMO energy level (affecting V_{oc}) and the band gap (deciding J_{sc}).

Experimental Section

Instrumentation. Microwave-assisted polymerizations were conducted in a CEM Discover Benchmate microwave reactor. Gel permeation chromatography (GPC) measurements of PNDT−4DTBT and PQDT−4DTBT were performed on (a) a Waters 2695 separations module apparatus with a differential refractive index detector with tetrahydrofuran (THF) as eluent and (b) a Polymer Laboratories PL-GPC 220 instrument (at the University of Chicago) using 1,2,4-trichlorobenzene as the eluent (stabilized with 125 ppm BHT) at 135 °C. The obtained molecular weight is relative to the polystyrene standard. An Asylum Research MFP3D atomic force microscope (AFM) was used for taking AFM images. Differential scanning calorimeter (DSC) curves were acquired with a TA Q200 instrument. ^{1}H nuclear magnetic resonance (NMR) measurements were recorded either with a Bruker Avance 300 MHz AMX or a Bruker 400 MHz DRX spectrometer. ^{13}C nuclear magnetic resonance (NMR) measurements were carried out with a Bruker 400 MHz DRX spectrometer. Chemical shifts were expressed in parts per million (ppm), and splitting patterns are designated as s (singlet), d (doublet), m (multiplet), and br (broad). Coupling constants J are reported in hertz (Hz).

Polymer Solar Cell Fabrication and Testing. Glass substrates coated with patterned indium-doped tin oxide (ITO) were purchased from Thin Film Devices, Inc. The 150 nm sputtered ITO pattern had a resistivity of 15 Ω/□. Prior to use, the substrates were ultrasonicated in acetone followed by deionized water and then 2-propanol for 20 min each. The substrates were dried under a stream of nitrogen and subjected to the treatment of UV-ozone over 30 min. A 0.45 μm filtered dispersion of PEDOT:PSS in water (Baytron PH500) was then spun-cast onto clean ITO substrates at 4000 rpm for 60 s and then baked at 140 °C for 15 min to give a thin film with a thickness of 40 nm. A blend of polymer and $PC_{61}BM$ with varied concentration and feed ratio were dissolved in dichlorobenzene with heating at 110 °C for 6 h. All the solutions were filtered through a 1 μm poly(tetrafluoroethylene) (PTFE) filter, spun-cast at different rpm for 60 s onto a PEDOT:PSS layer. The substrates were then dried under a nitrogen atmosphere at room temperature for 12 h. The thicknesses of films were recorded by a profilometer (Alpha-Step 200, Tencor Instruments). The devices were finished for measurement after thermal deposition of a 40 nm film of calcium and a 70 nm aluminum film as the cathode at a pressure of $\sim 1 \times 10^{-6}$ mbar. There were 8 devices per substrate, with an active area of 12 mm^2 per device. Device characterization was carried out under AM 1.5G irradiation with the intensity of 100 mW/cm^2 (Oriel 91160, 300 W) calibrated by a NREL certified standard silicon cell. Current density versus potential ($J-V$) curves were recorded with a Keithley 2400 digital source meter. IPCE were detected under monochromatic illumination (Oriel Cornerstone 260 1/4 m monochromator equipped with Oriel 70613NS QTH lamp), and the calibration of the incident light was performed with a monocrystalline silicon diode. All fabrication steps after adding the PEDOT:PSS layer onto ITO substrate, and characterizations were performed in gloveboxes under a nitrogen atmosphere.

Materials. All reagents and chemicals were purchased from commercial sources (Aldrich, Acros, Strem, Fluka) and used without further purification unless stated otherwise. Reagent grade solvents were dried when necessary and purified by distillation. Naphtho[2,1-*b*:3,4-*b*′]dithiophene (NDT) and dithieno[3,2-*f*:2′,3′-*h*]quinoxaline (QDT) were synthesized according to our previous paper with slightly modified procedures.[22] The synthesis of 4,7-di(4-(2-ethylhexyl)-2-thienyl)-2,1,3-benzothiadiazole was described elsewhere.[21,23]

4,7-Bis(5-bromo-4-(2-ethylhexyl)-2-thienyl)-2,1,3-benzothiadiazole (4DTBT). 4,7-Di(4-(2-ethylhexyl)-2-thienyl)-2,1,3-benzothiadiazole (0.86 g, 1.64 mmol) and *N*-bromosuccinimide (NBS) (641 mg, 3.60 mmol) were added into THF 150 mL under stirring. The reaction mixture was stirred at a room temperature for 6 h. The reaction mixture was then washed with brine and dried over anhydrous sodium sulfate. The solvent was removed under reduced pressure to give the product as a red solid. Needle-like crystals were obtained by recrystallization from ethanol. Yield: 1.02 g (91%). ^{1}H NMR (300 MHz, $CDCl_3$): δ 7.74 (s, 2H), 7.73 (s, 2H), 2.59 (m, 4H), 1.73 (m, 2H), 1.33−1.40 (m, 16H), 0.92 (m, 12H). ^{13}C NMR (400 MHz, $CDCl_3$): δ 152.20, 142.26, 138.35, 128.65, 125.37, 124.86, 112.26, 40.02, 33.94, 32.55, 28.81, 25.78, 23.06, 14.08, 10.86.

Synthesis of Polymers. PNDT−4DTBT and PQDT−4DTBT were synthesized via microwave-assisted Stille coupling polymerization shown in Scheme 1. A representative procedure is as follows. To a 10 mL microwave-pressurized vial equipped with a stirring bar, NDT (160 mg, 0.202 mmol), 4DTBT (138 mg, 0.202 mmol), $Pd_2(dba)_3$ (4.6 mg, 2.5%), and P(*o*-tol)$_3$ (12.7 mg, 20%) were added. Then the tube was sealed, evacuated, and refilled with argon for three cycles. Subsequently chlorobenzene (0.8 mL) was added into the same reaction tube inside a glovebox. Reaction tube was put into microwave reactor and heated to 150 °C under 300 W microwave for 20 min. After cooling to room temperature, the organic solution was added dropwise to 200 mL of methanol to obtain precipitate, which was collected by filtration and washed with methanol and dried. The crude polymer was then extracted subsequently with methanol, ethyl acetate, hexane, and $CHCl_3$ in a Soxhlet extractor. The fraction from chloroform was concentrated under reduced pressure and precipitated into methanol to give the polymer PNDT−4DTBT (151 mg, 76%) as a dark green solid.

PQDT−4DTBT was synthesized according to the same procedure as PNDT−4DTBT with respective monomers.

PNDT−4DTBT: ^{1}H NMR (400 MHz, $CDCl_2CDCl_2$, 400 K): δ 0.79−1.12 (24H, br), 1.27−1.67 (32H, br), 1.79−2.02 (4H, br), 2.83−3.09 (8H, br), 7.94 (2H, br), 7.99 (2H, br), 8.13 (2H, br), 8.19 (2H, br).

PQDT-4DTBT: ^{1}HNMR (400 MHz, $CDCl_2CDCl_2$, 400 K): δ 0.82−1.25 (24H, br), 1.27−1.83 (32H, br), 1.94 (2H,br), 2.32 (2H, br), 3.02 (4H, br), 3.11 (4H, br), 7.96 (2H, br), 8.08 (2H, br), 8.44 (2H, br).

Results and Discussion

Polymer Synthesis. Both polymers were synthesized by microwave-assisted Stille coupling reaction[11,24,25] of distannylated NDT or QDT and dibrominated 4DTBT as shown in Scheme 1. Identical alkyl chains (2-ethylhexyl) were

Scheme 1. Polymerization of PNDT−4DTBT and PQDT−4DTBT

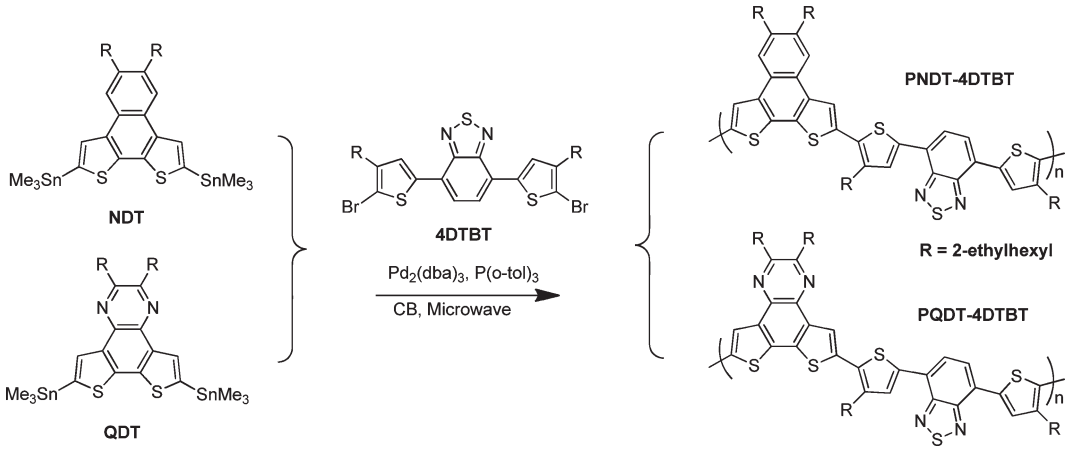

Table 1. Polymerization Results of PNDT−4DTBT and PQDT−4DTBT

polymer	M_n[a] [kg/mol]	PDI[a]	M_n[b] [kg/mol]	PDI[b]
PNDT−4DTBT	25.7	3.93	6.8	2.07
PQDT−4DTBT	12.9	2.26	5.2	1.90

[a] Determined by GPC in tetrahydrofuran (THF) using polystyrene standards. [b] Determined by high-temperature GPC using 1,2,4-trichlorobenzene as the eluent (stabilized with 125 ppm BHT) at 135 °C with polystyrene standards.

anchored on the PNDT−4DTBT and PQDT−4DTBT polymer backbones to avoid the possible chain effects on polymer properties.[26−29] Both polymers are readily soluble in common solvents such as chloroform, chlorobenzene (CB), and dichlorobenzene (DCB). The high solubility and high molecular weight of these two polymers highlight the benefits of incorporating a soluble acceptor (e.g., 4DTBT) in constructing low band gap polymers.[21] The structures of these purified polymers were confirmed by ^{1}H NMR (see Supporting Information). Gel permeation chromatography (GPC) results using tetrahydrofuran (THF) as eluent at room temperature and using 1,2,4-trichlorobenzene (TCB) at 135 °C are shown in Table 1. Molecular weights and polydispersity index (PDI) measured under high temperature and in good solvent are noticeably smaller than these values obtained in THF at room temperature. Furthermore, symmetrical curve with single peak in the GPC spectrum were obtained in the former condition whereas multiple peaks were shown in the latter condition. These different results from two different running conditions of GPC measurements indicate strong tangling and aggregation of these studied polymers at room temperature (see Supporting Information). We also investigated the thermal behavior of PNDT−4DTBT and PQDT−4DTBT through DSC analysis, which revealed no obvious thermal transitions in the temperature range from 10 to 150 °C.

Optical Properties. The absorption spectra of the polymers in chlorobenzene (CB) solution at different temperatures and in solid films are shown in Figure 2, and the related data are summarized in Table 2. Solution UV−vis spectra in CB solution at various temperatures showed similar absorption maximum for both PNDT−4DTBT and PQDT−4DTBT. In CB solution at room temperature, PNDT−4DTBT also showed signs of aggregation via strong interchain $\pi-\pi$ interaction, which is suggested by an additional absorption shoulder around 700 nm (Figure 2a). This absorption shoulder is much weaker in the absorption spectrum of PQDT−4DTBT, suggesting a reduced aggregation in PQDT−4DTBT. These additional absorption shoulders disappeared when the solution was heated to 100 °C. This observation indicated the breakup of these aggregates in good solvent at elevated temperature, which was corroborated by the GPC study. Absorption shoulder is more pronounced in the solid state for both polymers, indicating strong π-stacking and polymer chain reorganization.[11] Again, PNDT−4DTBT showed a further red shift, extending beyond 800 nm to the IR region. A band gap of 1.61 eV was estimated from the onset of the film absorption for PNDT−4DTBT, smaller than that of PQDT−4DTBT (1.70 eV). The narrower band gap should lead to more light absorption and a higher current.

Electrochemical Properties. Cyclic voltammograms were recorded from thin films of PNDT−4DTBT and PQDT−4DTBT drop-casted from chloroform solutions (see Supporting Information). The potentials were internally calibrated using the ferrocene/ferrocenium redox couple (Fc/Fc^+). The CV curves of both polymers are shown in Figure 3a, and the HOMO levels (calculated from onset of the oxidation peaks) and LUMO levels (calculated from the HOMO level and the optical band gap of each polymer) are illustrated in Figure 3b. Both electrochemical characterizations of polymer thin films via cyclic voltammetry (CV) and calculated using optical band gaps reveal that these two polymers share similar LUMO energy levels. This similarity is expected since the LUMO of donor−acceptor copolymers is largely determined by the acceptor moiety.[20,30] However, substituting naphthalene unit with more electron-deficient quinoxaline in the donor part weakens the electron-donating ability of QDT, leading to the observed lower HOMO energy level of −5.46 eV (PQDT−4DTBT) compared with −5.34 eV (PNDT−4DTBT) (Figure 3b). The difference of 0.12 eV in HOMO energy levels, together with a near identical LUMO energy level, explains the observed difference of 0.09 eV in the band gaps of PNDT−4DTBT and PQDT−4DTBT. The lower HOMO energy level suggests that a higher voltage can be obtained in the BHJ devices.

Computational Study. Computational studies of PNDT−4DTBT and PQDT−4DTBT provide insightful information to account for the observed difference of optical and electrochemical properties. To simplify the calculation, only one repeating unit of each polymer was subject to the calculation, with alkyl chains replaced by CH_3 groups. The simulated electron density distributions are shown in Figure 4, and the calculated HOMO and LUMO levels are listed in Table 2. The electron density distributions of LUMO levels for both polymers are nearly identical and both primarily localized on the 4DTBT unit. Thus, the change of donor units has little

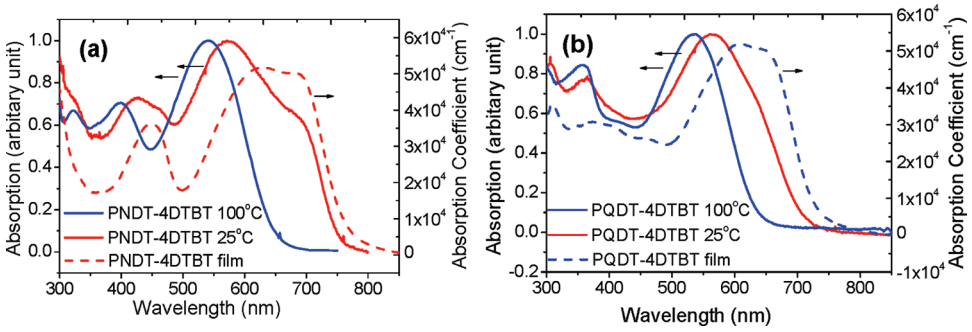

Figure 2. UV−vis absorption of PNDT−4DTBT (a) and PQDT−4DTBT (b) in various conditions: in chlorobenzene solution at 100 °C (blue solid line), at room temperature (red solid line), and in solid films (dotted line).

Table 2. Energy Levels and Optical Data of PNDT−4DTBT and PQDT−4DTBT

					UV−vis absorption				
					CB solution		film		
polymer	HOMO[a] [eV]	LUMO[a] [eV]	calcd HOMO[b] [eV]	calcd LUMO[b] [eV]	λ_{max}[c] [nm]	λ_{max}[d] [nm]	λ_{max} [nm]	λ_{onset} [nm]	E_g[e] [eV]
PNDT−4DTBT	−5.34	−3.29	−5.09	−2.86	573	540	629, 681	766	1.61
PQDT−4DTBT	−5.46	−3.28	−5.18	−2.86	563	533	609, 647	728	1.70

[a] HOMO and LUMO levels are estimated from the onset of the oxidation and reduction peaks of cyclic voltammograms, respectively. [b] HOMO and LUMO levels calculated by density functional theory (DFT). [c] Absorption maxima at room temperature. [d] Absorption maxima at 100 °C. [e] Calculated from the intersection of the tangent on the low energetic edge of the absorption spectrum with the baseline.

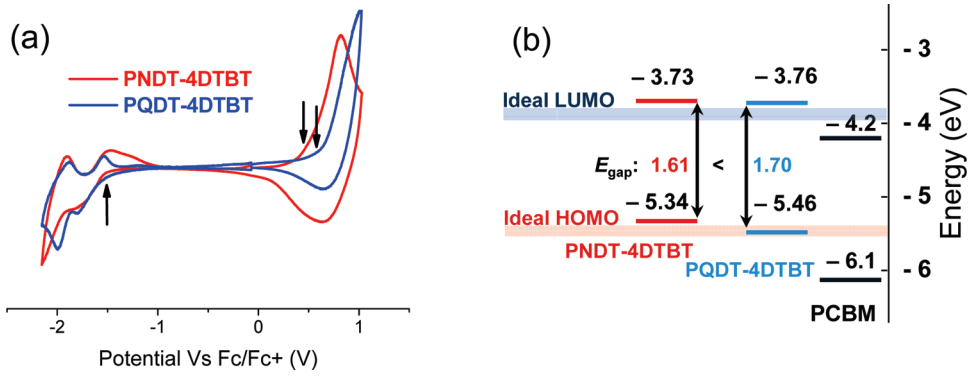

Figure 3. (a) Cyclic voltammograms of the oxidation and reduction behavior of PNDT−4DTBT and PQDT−4DTBT thin films. (The arrows indicate where the onsets of the oxidation and reduction peaks are. Note the LUMO levels of the two polymers are nearly identical.) (b) Energy band diagram. The LUMO level was calculated from the HOMO level and the optical band gap of each polymer. Ideal LUMO and HOMO levels were adapted from ref 3.

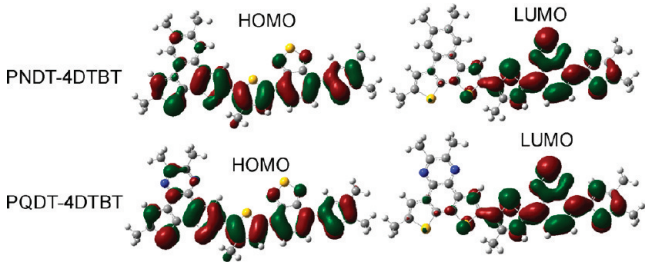

Figure 4. Simulated HOMO (left) and LUMO (right) electron density distributions of PNDT−4DTBT and PQDT−4DTBT by the DFT calculation.

effect on the LUMO levels. However, the electron density distributions of HOMO levels are delocalized, which indicates the donor unit significantly affects the HOMO level of the resulting polymer. By changing NDT unit to the "weaker donor" QDT unit, the calculated HOMO level of PQDT−4DTBT is decreased compared with that of PNDT−4DTBT. However, the LUMO level of PQDT−4DTBT is identical to that of PNDT−4DTBT since both polymers share the same acceptor unit, 4DTBT. The results from the calculation follow the same trend as we observed from the experimental values.

Photovoltaic Properties. Photovoltaic properties of both polymers were probed on typical BHJ solar cell with a configuration of ITO/PEDOT:PSS (40 nm)/polymer:$PC_{61}BM$/Ca (40 nm)/Al (70 nm). Representative $J-V$ curves are shown in Figure 5a, and their photovoltaic performances are summarized in Table 3. In the case of PNDT−4DTBT, a thin film of ∼95 nm were obtained by spin-coating a polymer:$PC_{61}BM$ (1:0.8 w/w) solution in DCB onto a PEDOT:PSS layer. The active layer of PQDT−4DTBT BHJ cells has a thickness of ∼85 nm, processed from a blend of polymer:$PC_{61}BM$ (1:1.2 w/w) in DCB. Indeed, the smaller band gap of PNDT−4DTBT produces a short circuit current of 14.20 mA/cm^2, which is one of the highest J_{sc} generated by polymer/$PC_{61}BM$ BHJ *without* applying any additives.[12,13] Along with an open circuit voltage of 0.67 V and a fill factor of 54.0%, a power conversion efficiency of 5.1% is achieved. Conversely, the lower HOMO energy level of PQDT−4DTBT translates into a much higher V_{oc} of 0.83 V. However, a lower

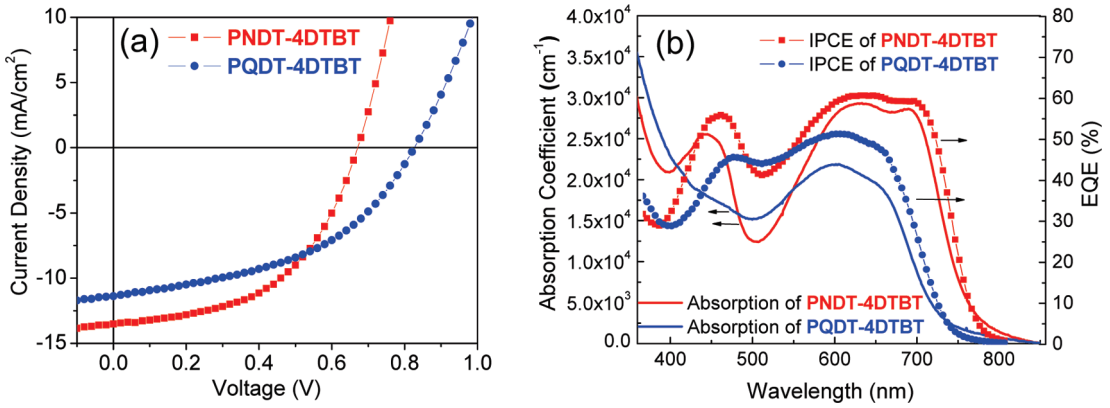

Figure 5. (a) Characteristic $J-V$ curves of the devices of polymer-based BHJ solar cells under 1 sun condition (100 mW/cm^2). (b) IPCE and absorption of semioptimized devices.

Table 3. Photovoltaic Performances of Polymers

polymer	polymer:$PC_{61}BM$	processing solvent	thickness (nm)	V_{oc} (V)	J_{sc} (mA/cm^2)	*FF* (%)	η (%)
PNDT−4DTBT	1:0.8	DCB	95	0.67	14.20	54.0	5.1
PQDT−4DTBT	1:1.2	DCB	85	0.83	11.38	45.6	4.3

Table 4. Mobility of Polymers under SCLC Conditions

	polymer only		polymer/$PC_{61}BM$ blend		
polymer	thickness (nm)	mobility (cm^2/V s))	polymer:$PC_{61}BM$	thickness (nm)	mobility (cm^2/V s))
PNDT−4DTBT	70	1.73×10^{-5}	1:0.8	95	7.17×10^{-5}
PQDT−4DTBT	45	7.24×10^{-6}	1:1.2	70	1.79×10^{-5}

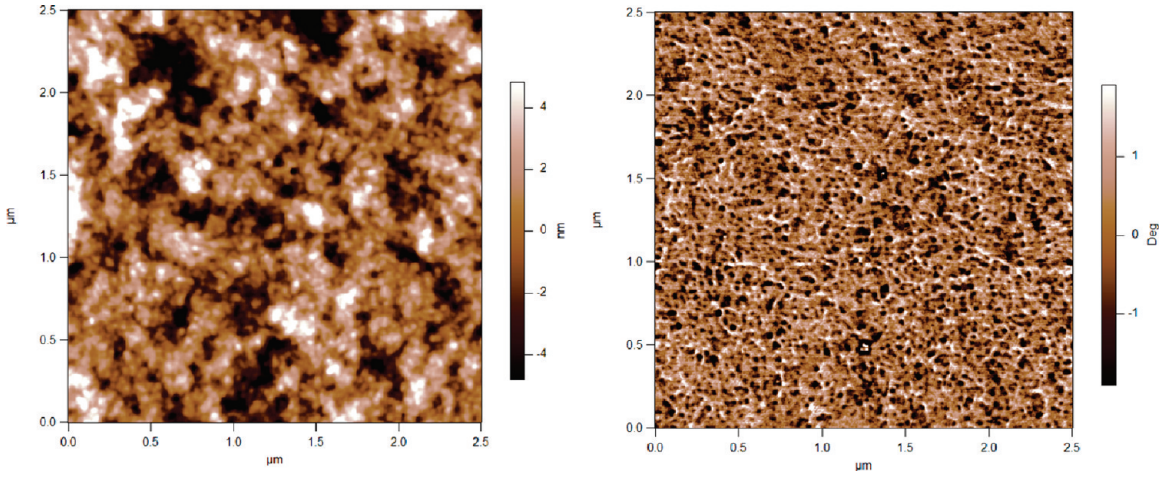

Figure 6. AFM images of PNDT−4DTBT:$PC_{61}BM$ film in a 1:0.8 ratio blend (left: height image; right: phase image).

J_{sc} of 11.38 mA/cm^2 was obtained, which can be largely attribute to the slightly larger band gap and smaller absorption coefficient of PQDT−4DTBT (Figure 5b). With a fill factor of 45.6%, a lower efficiency (4.3%) is obtained for PQDT−4DTBT-based devices.

Figure 5b shows the incident photo-to-current efficiency (IPCE) of related BHJ devices, together with their individual film absorption. Both BHJ devices show significant photo-to-current response in nearly the entire visible range (400−800 nm). For the PNDT−4DTBT/$PC_{61}BM$ solar cell, an IPCE of ~60% was observed spanning from 620 to 720 nm. Although the absorption band of PQDT−4DTBT is narrower because of a larger band gap, its BHJ solar cell still exhibits wide photo-to-current response with decent IPCE values over 40% from 450 to 680 nm. The calculated J_{sc} by integrating the spectral response of the cells agrees well with photocurrent obtained by $J-V$ measurements. Mobility measurements via space charge limited current (SCLC) are summarized in Table 4. A hole mobility of 7.17×10^{-5} cm^2/(V s) was observed for the PNDT−4DTBT:$PC_{61}BM$ device, more than double that of the PQDT−4DTBT:$PC_{61}BM$ device (1.79×10^{-5} cm^2/(V s)). The relatively low hole mobility partially explains why films thinner than 100 nm need to be employed in both cases.[30]

Device Morphology. The impact on the morphology by this small structural modification of similar polymers was studied using atomic force microscopy (AFM). Surface topography and phase images were acquired for each polymer/$PC_{61}BM$ film as shown in Figures 6 and 7, respectively. Relatively smooth surfaces with similar roughness observed for both polymer/$PC_{61}BM$ films suggest similar solubility of these two polymers in the processing solvent (DCB) due to the structural similarity of these two polymers with identical solubilizing alkyl chains. However, noticeable difference was

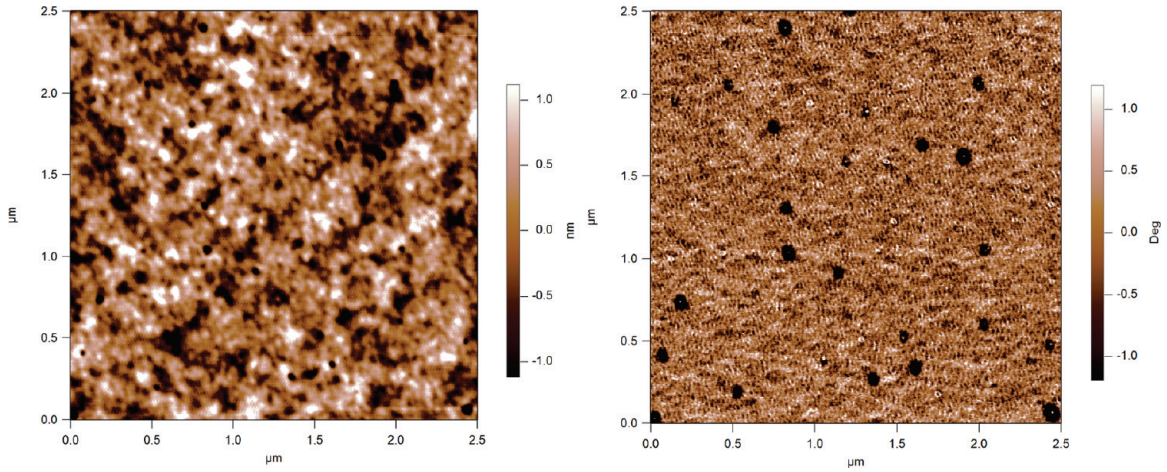

Figure 7. AFM images of PQDT−4DTBT:$PC_{61}BM$ film in a 1:1.2 ratio blend (left: height image; right: phase image).

observed in the phase images. Phase-separated domains of similar sizes can be clearly observed in the BHJ film of PNDT−4DTBT/$PC_{61}BM$, whereas no clear evidence of such phase separation was obtained in the blend film of PQDT−4DTBT/$PC_{61}BM$. The difference in the morphologies indicates a stronger interchain $\pi-\pi$ interaction in the case of PNDT−4DTBT than that in PQDT−4DTBT, which is consistent with the results of UV−vis spectra as previously discussed. A strong intermolecular $\pi-\pi$ interaction in the conjugated polymer/$PC_{61}BM$ blend typically correlates to a high short circuit current of BHJ solar cells (e.g., in widely studied P3HT solar cells[31−34]), which further supports the observed larger J_{sc} in the PNDT−4DTBT-based solar cell than in the case of PQDT−4DTBT.

Conclusions

In summary, we introduced two "weak donors", naphtho[2,1-*b*:3,4-*b*′]dithiophene (NDT) and dithieno[3,2-*f*:2′,3′-*h*]quinoxaline (QDT), to construct two "weaker donor−strong acceptor" polymers (PNDT−4DTBT and PQDT−4DTBT) with their conjugated backbones differing only by two atoms in the donor unit. Overall efficiencies of 5.1% and 4.3% have been achieved for PNDT−4DTBT- and PQDT−4DTBT-based BHJ devices in our preliminary photovoltaic studies. The subtle change on the donor unit leads to a pronounced effect on the HOMO energy level and the band gap of resulting polymers. Through these two polymers, we demonstrated that incorporating electron-withdrawing atoms in the *donor unit* would lead to a lower HOMO energy level, which would be beneficial to the V_{oc}; however, the LUMO level was much less affected by the electron-withdrawing atoms by the change in the donor unit. The concomitant enlargement of the band gap would lead to a smaller J_{sc}. Future research should be focused on employment of even weaker donor and stronger acceptors via innovative structural modification in order to *concurrently* achieve a higher V_{oc} and a higher J_{sc}. In the meantime, new strategies to further improve the hole mobility also need to be pursued.

Acknowledgment. This work was supported by the University of North Carolina at Chapel Hill, a DuPont Young Professor Award, Office of Naval Research (Grant N000140911016), and NSF CAREER Award (DMR-0954280). We thank Professor Richard Jordan and Mr. Zhongliang Shen of the University of Chicago for GPC characterization.

Supporting Information Available: Monomers and polymers NMR spectra; GPC curves; $J^{0.5}$ vs V plots of mobility measurement of polymers. This material is available free of charge via the Internet at http://pubs.acs.org.

References and Notes

(1) Dennler, G.; Scharber, M. C.; Brabec, C. J. *Adv. Mater.* **2009**, *21*, 1323.
(2) Chen, J.; Cao, Y. *Acc. Chem. Res.* **2009**, *42*, 1709.
(3) Thompson, B. C.; Fréchet, J. M. J. *Angew. Chem., Int. Ed.* **2008**, *47*, 58.
(4) Chen, H.-Y.; Hou, J.; Zhang, S.; Liang, Y.; Yang, G.; Yang, Y.; Yu, L.; Wu, Y.; Li, G. *Nat. Photonics* **2009**, *3*, 649.
(5) Liang, Y.; Xu, Z.; Xia, J.; Tsai, S.-T.; Wu, Y.; Li, G.; Ray, C.; Yu, L. *Adv. Mater.* **2010**, *22*, E135.
(6) Scharber, M. C.; Mühlbacher, D.; Koppe, M.; Denk, P.; Waldauf, C.; Heeger, A. J.; Brabec, C. J. *Adv. Mater.* **2006**, *18*, 789.
(7) Park, S. H.; Roy, A.; Beaupre, S.; Cho, S.; Coates, N.; Moon, J. S.; Moses, D.; Leclerc, M.; Lee, K.; Heeger, A. J. *Nat. Photonics* **2009**, *3*, 297.
(8) Zhang, F.; Jespersen, K. G.; Björström, C.; Svensson, M.; Andersson, M. R.; Sundström, V.; Magnusson, K.; Moons, E.; Yartsev, A.; Inganäs, O. *Adv. Funct. Mater.* **2006**, *16*, 667.
(9) Zheng, Q.; Jung, B. J.; Sun, J.; Katz, H. E. *J. Am. Chem. Soc.* **2010**, *132*, 5394.
(10) Wang, E.; Wang, L.; Lan, L.; Luo, C.; Zhuang, W.; Peng, J.; Cao, Y. *Appl. Phys. Lett.* **2008**, *92*, 033307.
(11) Coffin, R. C.; Peet, J.; Rogers, J.; Bazan, G. C. *Nat. Chem.* **2009**, *1*, 657.
(12) Liang, Y.; Wu, Y.; Feng, D.; Tsai, S.-T.; Son, H.-J.; Li, G.; Yu, L. *J. Am. Chem. Soc.* **2009**, *131*, 56.
(13) Liang, Y.; Feng, D.; Wu, Y.; Tsai, S.-T.; Li, G.; Ray, C.; Yu, L. *J. Am. Chem. Soc.* **2009**, *131*, 7792.
(14) Zhou, H.; Yang, L.; Price, S. C.; Knight, K. J.; You, W. *Angew. Chem., Int. Ed.* **2010**, *49*, 7992.
(15) Huo, L.; Hou, J.; Zhang, S.; Chen, H.-Y.; Yang, Y. *Angew. Chem., Int. Ed.* **2010**, *49*, 1500.
(16) Wienk, M. M.; Turbiez, M.; Gilot, J.; Janssen, R. A. J. *Adv. Mater.* **2008**, *20*, 2556.
(17) Chen, C.-P.; Chan, S.-H.; Chao, T.-C.; Ting, C.; Ko, B.-T. *J. Am. Chem. Soc.* **2008**, *130*, 12828.
(18) Blouin, N.; Michaud, A.; Gendron, D.; Wakim, S.; Blair, E.; Neagu-Plesu, R.; Belletete, M.; Durocher, G.; Tao, Y.; Leclerc, M. *J. Am. Chem. Soc.* **2008**, *130*, 732.
(19) Brabec, C. J.; Shaheen, S. E.; Fromherz, T.; Padinger, F.; Hummelen, J. C.; Dhanabalan, A.; Janssen, R. A. J.; Sariciftci, N. S. *Synth. Met.* **2001**, *121*, 1517.
(20) Zhou, H.; Yang, L.; Stoneking, S.; You, W. *ACS Appl. Mater. Interfaces* **2010**, *2*, 1377.
(21) Zhou, H.; Yang, L.; Xiao, S.; Liu, S.; You, W. *Macromolecules* **2010**, *43*, 811.
(22) Xiao, S.; Zhou, H.; You, W. *Macromolecules* **2008**, *41*, 5688.
(23) Price, S. C.; Stuart, A. C.; You, W. *Macromolecules* **2010**, *43*, 4609.
(24) Nehls, B. S.; Asawapirom, U.; Fuldner, S.; Preis, E.; Farrell, T.; Scherf, U. *Adv. Funct. Mater.* **2004**, *14*, 352.
(25) Galbrecht, F.; Bunnagel, T. W.; Scherf, U.; Farrell, T. *Macromol. Rapid Commun.* **2007**, *28*, 387.

(26) Piliego, C.; Holcombe, T. W.; Douglas, J. D.; Woo, C. H.; Beaujuge, P. M.; Fréchet, J. M. J. *J. Am. Chem. Soc.* **2010**, *132*, 7595.
(27) Hou, J.; Chen, T. L.; Zhang, S.; Huo, L.; Sista, S.; Yang, Y. *Macromolecules* **2009**, *42*, 9217.
(28) Gadisa, A.; Oosterbaan, W. D.; Vandewal, K.; Bolsée, J.-C.; Bertho, S.; D'Haen, J.; Lutsen, L.; Vanderzande, D.; Manca, J. V. *Adv. Funct. Mater.* **2009**, *19*, 3300.
(29) Yang, L.; Zhou, H.; You, W. *J. Phys. Chem. C* **2010**, *114*, 16793.
(30) Xiao, S.; Stuart, A. C.; Liu, S.; You, W. *ACS Appl. Mater. Interfaces* **2009**, *1*, 1613.
(31) Osaka, I.; McCullough, R. D. *Acc. Chem. Res.* **2008**, *41*, 1202.
(32) Li, G.; Yao, Y.; Yang, H.; Shrotriya, V.; Yang, G.; Yang, Y. *Adv. Funct. Mater.* **2007**, *17*, 1636.
(33) Li, G.; Shrotriya, V.; Yao, Y.; Huang, J.; Yang, Y. *J. Mater. Chem.* **2007**, *17*, 3126.
(34) Shin, M.; Kim, H.; Park, J.; Nam, S.; Heo, K.; Ree, M.; Ha, C.-S.; Kim, Y. *Adv. Funct. Mater.* **2010**, *20*, 748.